Imperfect Oriented Attachment: Accretion and Defect Generation of Hexagonal Inorganic-Surfactant Nanoparticles

ARTICLE *in* NANO LETTERS · JUNE 2001

Impact Factor: 13.59 · DOI: 10.1021/nl010020e

3 AUTHORS, INCLUDING:

Pouyan Shen
National Sun Yat-sen University
247 PUBLICATIONS **2,637** CITATIONS
SEE PROFILE

An-Chung Su
National Tsing Hua University
96 PUBLICATIONS **1,974** CITATIONS
SEE PROFILE

NANO LETTERS

2001
Vol. 1, No. 6
299−303

Imperfect Oriented Attachment: Accretion and Defect Generation of Hexagonal Inorganic-Surfactant Nanoparticles

P. Shen,* Y. Y. Fahn,† and A. C. Su

Institute of Materials Science and Engineering, National Sun Yat-sen University, Kaohsiung 804, Taiwan, R.O.C.

Received March 15, 2001 *(Revised Manuscript Received May 2, 2001)*

ABSTRACT

Imperfect oriented attachment of nanoparticles over specific surfaces is rationalized to cause accretion and defects for the hexagonal inorganic-surfactant mesophase. Analytical electron microscopy indicates that silicate MCM-41 particles, prepared in alkaline hydrothermal condition and then surfactant (cetyltrimethylammonium bromide) leached, have well-developed {10} surfaces with monolayer steps and a rather uniform base with constant tubular wall thickness. These surfaces are beneficial to {∼10} vicinal and head-on attachment, causing respectively edge dislocation and twist boundary for hexagonal silicatropic liquid crystal. Brownian motion may proceed above a critical temperature for anchorage release at the interface of imperfectly attached particles until an epitaxial relationship is reached.

A crystal in terms of 3-D ordering of atoms was recently proved to generate dislocations by imperfect oriented attachment on a specific atomic plane of nanoparticles,[1] whereas homogeneous single crystals separated by twin boundaries or another planar defect via oriented attachment on such planes.[2,3] As for liquid crystals (including inorganic-encased mesophases), it was not previously realized to have specific low-energy surfaces for analogous attachments.

In this report we describe accretion and defect generation of hexagonal inorganic-surfactant mesophase in terms of attachment over specific surfaces of colloidal nanoparticles. This view is based on the scrutiny of the defects and shape of silicate-encased and surfactant-leached particles of MCM-41 with 2-D crystal symmetry (plane group *p*6*mm*). (MCM-41 refers to Mobil Composition Material with a hexagonal array of uniform mesopores.[4]) Formation of this mesoporous molecular sieve involves a liquid crystal mechanism based on morphological[5] and in situ X-ray diffraction observations.[6] The hexagonal silicatropic liquid crystal (SLC, those that form in the presence of charged silicate oligomers, as pertinent to the production of MCM-41 material[7]), was generally accepted to derive from a lamellar phase[8] or disordered intermediate.[9] We suggest that regardless of its variable pathways, the hexagonal SLC once formed may accrete by Brownian motion and reorient impinged colloidal particles until an energetically favored state is reached.

To prepare the aluminosilicate MCM-41, 0.06 g of sodium aluminate (54% Al_2O_3; Riede-de Haën, Germany) was dissolved in 6.0 g of distilled water and this solution was mixed with 60.0 g of a 12% CTAB (cetyltrimethylammonium bromide, 99%; Merck) aqueous solution. Then 10.6 g of sodium silicate (27% SiO_2 and 14% NaOH; Aldrich) was added to the above solution. After the resulting mixture was stirred for 60 min at room temperature, 13.0 g of 1.0 M H_2SO_4 solution was slowly added by pipet for a total time of about 120 min. The gel mixture formed after this acidification step with pH adjusted to 10 was allowed to stand for 60 min and then was heated at 100 °C for 72 h in an oven. The solid product recovered by filtration was washed with deionized water, and ultrasonically vibrated and washed with ethanol. Suction on a Buchner funnel and filtration with 20-mesh filter paper was then employed to obtain MCM-41 particulates. This route has been successful in the synthesis of tubules-within-a-tubule in addition to particulates with silica or aluminosilicate wall.[10] We followed this procedure except a lower Al/Si ratio was adopted and the template was removed by ethanol rinsing to minimize possible effects of calcination on defect microstructures.

The synthesized powders before and after template removal were studied by X-ray diffraction (XRD using Siemens D5000 instrument at 40 kV, 30 mA with Cu Kα radiation) in the 2θ range 1−30° for the confirmation of a single phase of MCM-41 and the determination of its tubular interspacing. It turned out to be 4.9 nm based on $2/\sqrt{3}$ times the *d* spacing of diffraction peak (10) (Figure 1), i.e.,

* To whom correspondence should be addressed. Fax: 886-7-5254099. E-mail pshen@mail.nsysu.edu.tw.

† Present address: Department of Chemical Engineering, Eastern College of Technology and Commerce, Hu-Nei, Kaohsiung 829, Taiwan, R.O.C.

10.1021/nl010020e CCC: $20.00
Published on Web 06/13/2001

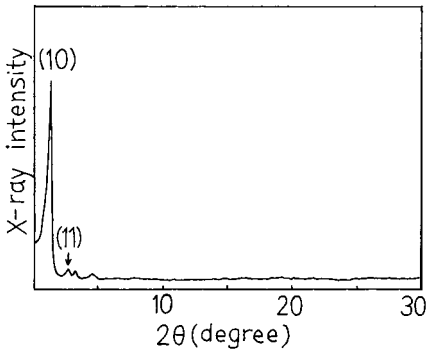

Figure 1. Powder X-ray diffraction pattern of silicate MCM-41 prepared in alkaline hydrothermal condition and after ethanol rinsing to remove CTAB. The patterns were measured on a diffractometer with Cu Kα radiation (wavelength = 0.154 nm). Indexed according to 2-D Miller indices (*hk*).

$(10\bar{1})$ in the (*hki*) indexing scheme; the removal of template was essentially complete, as indicated by the absence of a lamellar mesophase that otherwise exists before template removal. (2-D Miller indices (*hk*) were used to index the diffraction peaks of the hexagonal mesophase with plane group *p*6*mm*.) Template-cleaned powders were also dispersed in acetone and settled on a C-coated collodion film supported by Cu grid for the present analytical electron microscopic (AEM) characterization of defect microstructures and habit plane of MCM-41 nanoparticles that shed light on specific assembly mechanism of hexagonal mesophase. We used a JEOL 3010 instrument at 300 kV for imaging, electron diffraction, and point-count energy-dispersive X-ray (EDX) analysis of the sample. The selected area electron diffraction (SAED) patterns and images of nanoparticles were taken at various magnifications for the identification of lattice imperfections and shape, in particular, the habit plane, steps, and ledges that affect the coalescence behavior.

AEM-EDX analysis of surfactant-leached particles indicated the amorphous silicate wall consists of slight Al and much less Na. The Al is six-oxygen coordinated in the silicate network according to ^{27}Al MAS NMR data of the as-synthesized mesophase.[10] The silicate anions, but not aluminate anions, are the key counterions to cause condensation of the micellar surface according to room-temperature dynamic scattering and rheological characteristics that are highly sensitive to structural changes in polydisperse surfactant micelle systems.[11]

Transmission electron microscopic observations showed faceted MCM-41 particles ranging from nanometer to micrometer in size (Figure 2A). Regardless of the varied extent of assembly and coalescence to different sizes and thicknesses, the particles tend to have a hexagonal shape with uniform tubular diameters and wall thicknesses. A trigon as small as three tubules was also recognized on top of the particle to the left of Figure 2A (see also the enlarged view in Figure 3). The typical hexagons have well-developed {10} surfaces, as indicated by the configuration of tubules in the image at a higher magnification and corresponding electron diffraction pattern of the coalesced particles (Figure 2B). The {10} monolayers and their ledges commonly caused zigzag

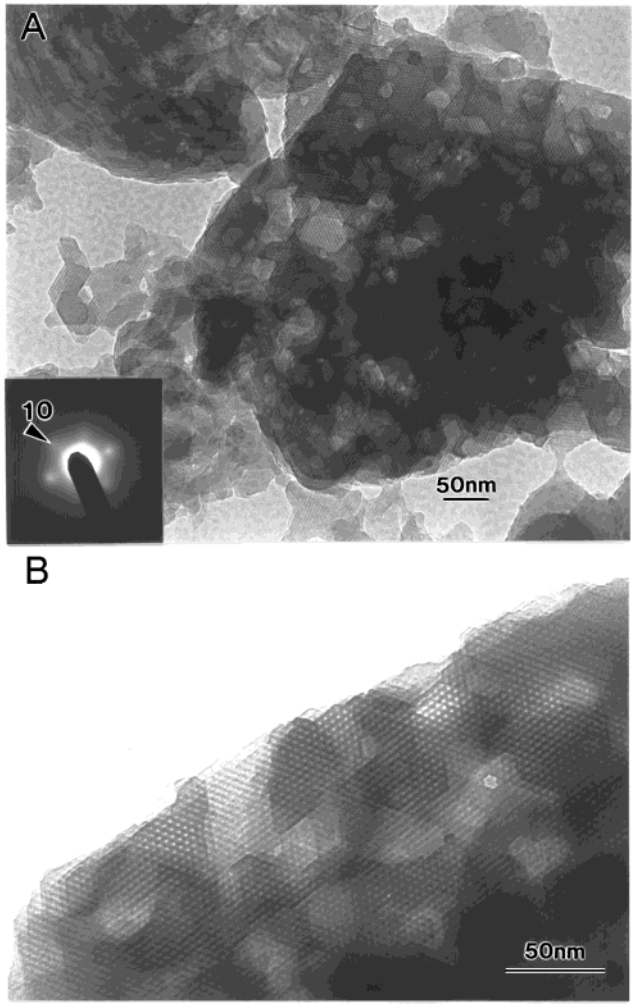

Figure 2. Transmission electron micrographs of silicate MCM-41 with template CTAB removed by ethanol. (A) Bright field image and inset selected area electron diffraction pattern of columnar hexagon colony (right), which is thicker than the yet to be coalesced nanometer-size particles (left). (B) Bright field image at a higher magnification of another colony with regular tubular wall thickness and monolayered {10} surfaces. The micrographs were taken at on a JEOL3010 microscope with an accelerating voltage of 300 kV.

{∼10} vicinal surfaces. Edge dislocation with the half-plane arrowed and depicted schematically (inset A) in Figure 4 can be accounted for by impingement of the hexagonal nanoparticles over such surfaces as discussed later. The columnar hexagons have rather flat bases for head-on attachment, leaving a twist boundary at the interface, as also shown in the top view in Figure 4 and schematically drawn as inset B with misorientation angle ϕ labeled. Regions near arrows A and B in Figure 4 are further magnified in Figure 5 for a clearer view of the edge dislocation with the half-plane edge-on and the twist boundary in plan view. Hexagonal pits or pores were commonly left over in the colony of such columnar hexagon modules (Figures 2 and 4). This is in accordance with the previous suggestion that the impingement of physically distinct domains of materials may result in pits as they grow in size through accretion,[12] although densification through two pathways, i.e., ordering into SLC and continued silicate polymerization,[13] may also cause pits.

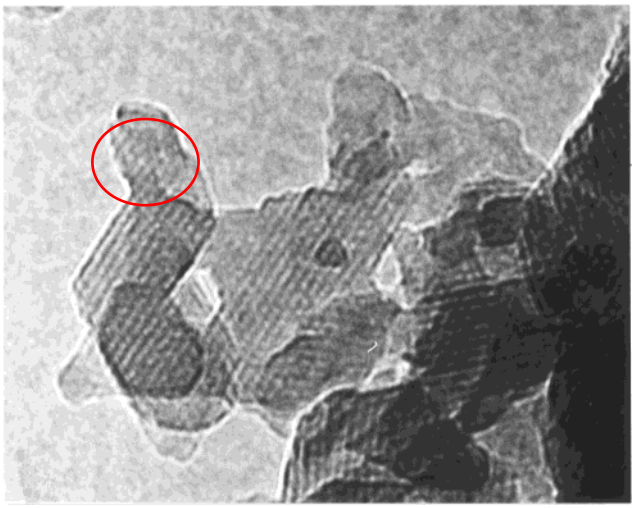

Figure 3. Further magnified view of the central-left region in Figure 2A to show hexagons and a trigon on top of a faceted and columnar hexagonal colony of silicate MCM-41. The tubular interspacing is ca. 5 nm.

Spherical particles with disordered mesopores likely due to entanglement of micelles under semidilute conditions were also observed in Figure 4. Under high pH, the silica particles are negatively charged and repel each other.[14] However, the charge-screening effect of the cationic surfactant enables the silicate-surfactant spherical particle to coalesce with the hexagonal particle, causing significantly stepwise yet uniformly walled {10} monolayers fading into a disordered necking area (Figure 4). Sintering-induced surface diffusion of silicate-encased rodlike micelles along the {10} plane is analogous to surface diffusion of atoms along {111} planes of sintered CeO_2 octahedra causing also amorphization near the necking area.[3] The room-temperature collective diffusion coefficient of flexible wormlike, yet silicate-encased, micelle was estimated by dynamic light scattering to be 10^{-6} to 10^{-7} $cm^2\ s^{-1}$ in the semidilute regime.[11] A temperature as high as 100 °C in the present case is presumably adequate to activate surface diffusion of micelles in the SLC regime. Relatively small columnar hexagons and trigons may attach randomly yet more effectively onto large spherical particles, forming protuberances with facets and tubules barely visible except edge-on (Figure 4).

The columnar MCM-41 colony as revealed in above TEM images can be rationalized by the assembly of a hexagonal module consisting of a hexagonal array of silicate-incorporated rodlike micelles and with well-developed {10} and {∼10} vicinal surfaces orthogonal to a more or less flat base (Figure 6). The rodlike micelles were already incorporated with oligomeric silicate species via ion exchange with counterions such as Br^- near the headgroup of the surfactant, before being assembled into hexagonal SLC. This is indicated by in situ small-angle neutron diffraction and deuterium NMR investigation of a dilute CTAB−H_2O solution with and without dissolved silica, showing that the addition of silicate solution to the micellar surfactant solution induced the formation of a hexagonal SLC.[7] Furthermore, their solid-state ^{29}Si magic-angle spinning (MAS) NMR spectrum indicates the D4R oligomer is the predominant multiply

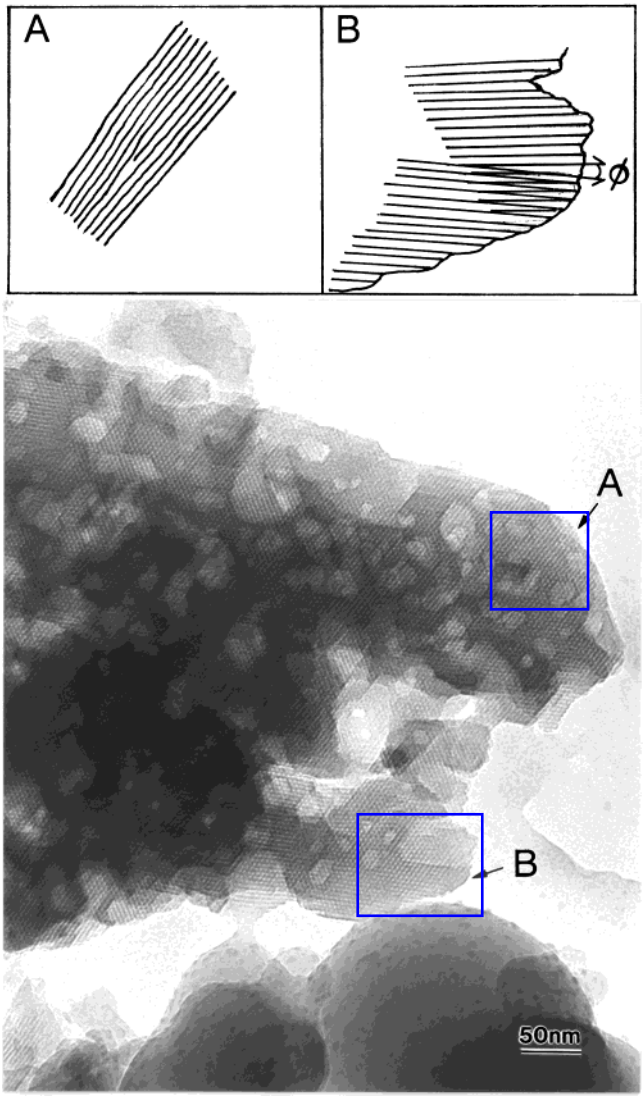

Figure 4. Transmission electron micrograph (bright field image) of the silicate MCM-41 colony from the same sample in Figure 2 showing edge dislocation and a twist boundary (depicted schematically as insets A and B, respectively; cf. also Figure 5) and faceted pits and pores among coalesced hexagonal particles. Also shown are two relatively large spherical particles with adjoined hexagons causing a disordered necking area (left) and protrusions (right) of the spherical surface.

charged silicate anion for multidentate interaction of a headgroup and interfacial silicate condensation is negligible. (High-temperature annealing of the solution or calcination, however, caused a more ordered polymerized silicate structure.) This multidentate bonding screens the intra-aggregate electrostatic headgroup repulsions among adjacent amphiphilic molecules, thereby reducing the average headgroup area, a_o, favorable to the spherical−cylindrical micelle transition.[15]

Perfect attachment of such modules on the {10} surface generated a homogeneous single crystal analogous to the case of the 3-D crystal,[2,3] although twinning is prohibited in the present 2-D case due to lack of polarity or other symmetry selection along the longitudinal direction of the tubules (Figure 6A). Steps may remain for this type of impingement to reconcile. Imperfect attachment on a {∼10} vicinal

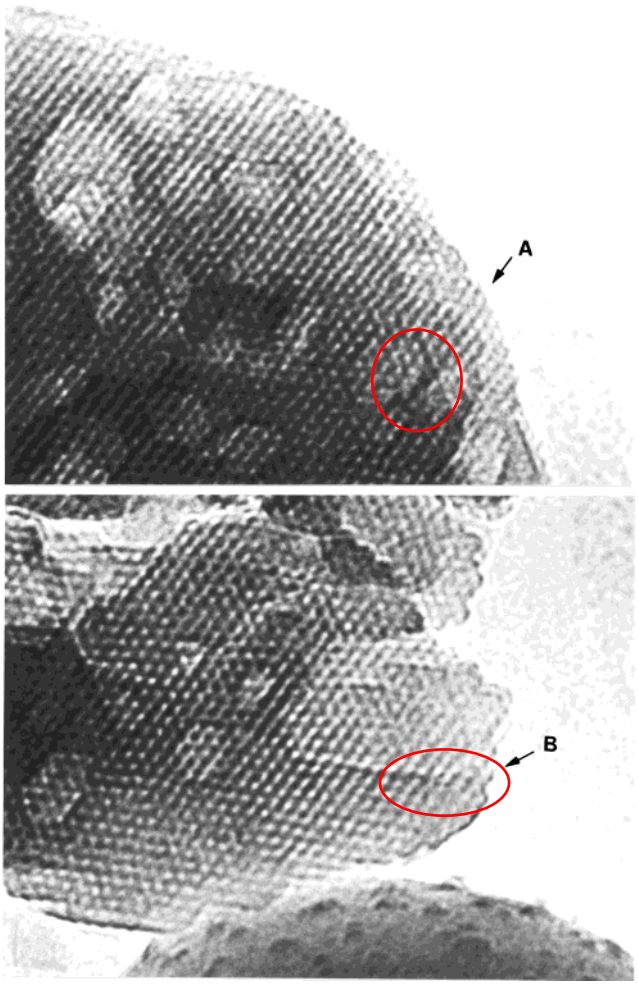

Figure 5. Further magnified regions near arrows A and B in Figure 4 to show the edge dislocation and twist boundary. The tubular interspacing is ca. 5 nm.

surface, as shown representatively in Figure 6B for the case of {10}/{11} joined with a specified misorientation ϕ of 30°, causes edge dislocation with the extra half-plane perpendicular to Burgers vector. The head-on attachment over the base of the modules may involve variable {10} plane misorientations, causing a twist boundary to various extents (Figure 6C). Pits and pores can be left over when the colony of such modules becomes larger (Figure 6D).

A perfect oriented attachment relies on the specific flat surface of the particles. In general, a plane with close-packed rows of atoms is energetically favored for 3-D crystals according to the periodic bond chain model.[16] The {10} plane of the present SLC hexagons is also close-packed in terms of silicate-encased tubules. This tubular habit plane is in accordance with a staggered minimum-energy fracture plane according to freeze-fracture TEM observation.[7] The columnar hexagon base is rather flat due to a rather quick self-alignment of silicate-encased rodlike micelles, with a specific aspect ratio above a critical micelle concentration,[15] attached to the nucleus, possibly a nanometer-size trigon (cf. Figure 3), to minimize surface steps of the particle. As to interfacial energy cusp, it generally refers to surface and strain energies for inorganic crystals. In the present case of adjoined

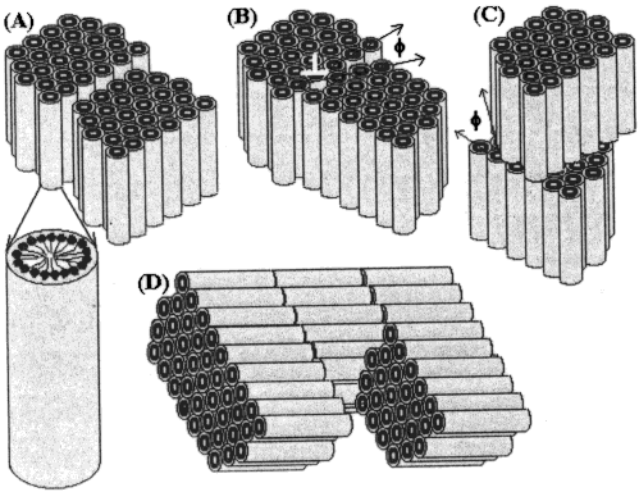

Figure 6. Schematic diagram of the accretion model in terms of variable attachments of hexagonal SLC modules. (A) Perfect attachment over {10} surface yet with steps left. (B) Imperfect attachment on {10}/{∼10} causing edge dislocation at the interface. (C) Imperfect head-on attachment over the module base causing twist boundary. (D) Assembly of a number of such modules to form pits and pores.

hexagonal SLC modules, interfacial multidentate interactions pertinent to the electrostatic and steric effect of both the surfactant and inorganic may play an important role in the energetics. A rather uniform tubular wall thickness and flat base presumably takes less effort for the reorientation of head-on attached modules in terms of the alignment of both surfactant molecules and silicate skeletons when imperfectly attached. It seems that the cohesive energy per unit area would be very different (larger) for the TiO_2 and Fe_2O_3 nanocrystals studied by Banfield et al.,[1,2] than for the case of the mesoporous structures studied here. This would imply a lower density of imperfect attachments for a given time/temperature/size in the present case.

The reorientation of the imperfectly impinged modules requires thermally activated Brownian migration and rotation of hexagonal SLC particles in addition to silicate-encased micelles. In fact, Brownian motion proceeds in solution, on a substrate, and even in the bulk. The so-called "Brownian movement" was described for the first time by the botanist Robert Brown who observed that the pollen of different plants became dispersed in water in a great number of small particles, which were perceived to be in uninterrupted and irregular "swarming" motion.[17] The first precise investigations of Brownian movement, however, are due to Prof. Gouy (of Lyons), who found that the motion is more lively the smaller the viscosity of the liquid is.[18] Einstein later proved that the movements of the particles suspended in liquids are demanded by the molecular theory of heat.[19] Brownian motion of crystallites was proved experimentally[20] and theoretically[21,22] to occur over a single-crystal surface. And the contact plane specification was commented to cause the epitaxy-orientation bifurcation of the crystallites.[23] Analogous motion was also found along the surface step[24] and in composite prepared via a sintering route.[25−27] In general, it requires $T/T_m > 0.8$ (where T_m is the melting temperature in Kelvin) for the anchorage release at the interphase interface

and viscous motion in terms of atom diffusion along the interface. Under such a condition, the migration−rotation of intragranular particles may reach epitaxy orientations with respect to its host grain.

In all cases, the mobility increases exponentially with the increase of temperature but decreases exponentially with particle size. It has been proved experimentally by Métois and colleagues that nanometer-size face-centered cubic metal particles such as Au can migrate and coalesce on KCl(100) substrate at 94 °C by anchorage release, i.e., debonding of atoms at the interface.[20] Thus, nanometer-size columnar hexagonal SLC modules are expected to move upon imperfect attachment in a solution heated to 100 °C, as in the present case. The motion, however, becomes difficult at a larger size, leaving imperfections in the columnar colony.

We are proposing a mechanism for the growth and defect structures of the hexagonal inorganic−surfactant mesophase in terms of Brownian motion above a critical temperature for anchorage release at the interface of imperfectly attached particles until an epitaxial relationship is reached. The well-developed {10} surfaces with monolayer steps and a rather uniform base with constant tubular wall thickness are beneficial to {∼10} vicinal and head-on attachment, causing respectively edge dislocation and a twist boundary for a hexagonal silicatropic liquid crystal. This mechanism is in accordance with the deposition of self-assembled rodlike silicate micelles into macroscopic hexagonal, and hence perfectly attached, MCM-41 particles when prepared at a specified TEOS concentration.[28] Further study is required to find out if this mechanism can be extended to other pH conditions and template types. It is also an open question whether this pathway can be generalized to the synthesis of other nonsiliceous materials as well as microorganisms with hexagonal skeleton[29,30] or gas vesicles[31] imperfectly assembled as colonies.

References

(1) Penn, R. L.; Banfield, J. F. *Science* **1998**, *281*, 969.
(2) Penn, R. L.; Banfield, J. F. *Am. Mineral.* **1998**, *83*, 1077.
(3) Lee, W. S.; Shen, P. *J. Cryst. Growth* **1999**, *205*, 169.
(4) Kresge, C. T.; Leonowicz, M. E.; Roth, W. J.; Vartuli, J. C.; Beck, J. S. *Nature* **1992**, *359*, 701.
(5) Cheng, C. F.; He, H.; Zhou, W.; Klinowski, J. *Chem. Phys. Lett.* **1995**, *244*, 117.
(6) Rathousky, J.; Schulzekloff, G.; Had, J.; Zukal, A. *Phys. Chem. Chem. Phys.* **1999**, *1*, 3053.
(7) Firouzi, A.; Kumar, D.; Bull, L. M.; Besier, T.; Sieger, P.; Huo, Q.; Walker, S. A.; Zasadzinski, J. A.; Glinka, C.; Nicol, J.; Margolese, D.; Stucky, G. D.; Chmelka, B. F. *Science* **1995**, *267*, 1138.
(8) Monnier, A.; Schüth, F.; Huo, Q.; Kumar, D.; Margolese, D.; Maxwell, R. S.; Stucky, G. D.; Krishnamurty, M.; Petroff, P.; Firouzi, A.; Janicke, M.; Chmelka, B. F. *Science* **1993**, *261*, 1299.
(9) Brown, A. S.; Holt, S. A.; Dam, T.; Trau, M.; White, J. W. *Langmuir* **1997**, *3*, 66363.
(10) Lin, H. P.; Mou, C. Y. *Science* **1996**, *273*, 765.
(11) Lee, Y. S.; Surjadi, D.; Rathman, J. F. *Langmuir* **1996**, *12*, 6202.
(12) Yang, H.; Coombs, N.; Dag, O.; Sokolov, I.; Ozin, G. A. *J. Mater. Chem.* **1997**, *7*, 1755.
(13) Yao, N.; Ku, A. Y.; Nakagawa, N.; Lee, T.; Saville, D. A.; Aksay, I. A. *Chem. Mater.* **2000**, *12*, 1536.
(14) Iler, R. K. *The Chemistry of Silica Solubility, Polymerization, Colloid and Surface Properties, and Biochemistry*; John Wiley & Sons: New York, 1979; p 866.
(15) Israelachvili, J. N.; Mitchell, D. J.; Ninham, B. W. *J. Chem. Soc., Faraday Trans. 2* **1976**, *72*, 1525.
(16) Hartman, P. Modern PBC Theory. In *Morphology of Crystals, Part A*; Sunagawa, I., Ed.; Terra Science and D. Reidel Co: Tokyo, 1987; p 271.
(17) Brown, R. *Philos. Mag.* **1828**, *4*, 161.
(18) Gouy, M. *J. Phys.* **1888**, *7*, 561.
(19) Einstein, A. *Ann. Phys.* **1905**, *17*, 549; **1906**, *19*, 371.
(20) Masson, A.; Métois, J. J.; Kern, R. *Surf. Sci.* **1971**, *27*, 463.
(21) Kern, R.; Masson, A.; Métois, J. J. *Surf. Sci.* **1971**, *27*, 483.
(22) Métois, J. J.; Gauch, M.; Masson, A.; Kern, R. *Surf. Sci.* **1972**, *30*, 43.
(23) Kuo, L. Y.; Shen, P. *Surf. Sci.* **1997**, *373*, L350.
(24) Métois, J. J. *Surf. Sci.* **1973**, *36*, 269.
(25) Chen, J.; Shen, P. *Scr. Mater.* **1997**, *37*, 1287.
(26) Wang, S. R.; Shen, P. *Mater. Sci. Eng.* A **1998**, *251*, 106.
(27) Lin, K. T.; Shen, P. *Mater. Sci. Eng.* A **1999**, *270*, 125.
(28) Cai, Q.; Luo, Z. S.; Pang, W. Q.; Fan, Y. W.; Chen, X. H.; Cui, F. Z. *Chem. Mater.* **2001**, *13*, 258.
(29) Thompson, D. W. *On Growth and Form−The complete revised edition*; Dover: New York, 1992; p 1116.
(30) Arduini, P.; Teruzzi, G. *Guide to Fossils*; Simon and Schuster: New York, 1986.
(31) Walsby, A. E. *Microbiol. Rev.* **1994**, *58*, 94.

NL010020E